Comparative Medicine
Copyright 2018
by the American Association for Laboratory Animal Science

Vol 68, No 3
June 2018
Pages 233–238

Case Study

Superparamagnetic Iron Oxide-enhanced Magnetic Resonance Imaging of Spontaneous Hepatic Neoplasia in a Cynomolgus Macaque (*Macaca fascicularis*)

Yasuyo Ito Fujishiro,[1,2] Hiroshi Koie,[2] Shunya Nakayama,[1,2] Hiroaki Shibata,[1] Sachi Okabayashi,[3] Yuko Katakai,[3] Kiichi Kanayama,[2] Yasuhiro Yasutomi,[1] and Naohide Ageyama[1,*]

Although the number of reports describing tumors in aged NHP has increased, spontaneous neoplasias in NHP are extremely rare, with the notable exception of prosimians, in which spontaneous hepatic neoplasms arise. In addition to radiography and ultrasonography, superparamagnetic iron oxide (SPIO)-enhanced MRI tends to be applied in human practice to noninvasively locate, identify, and size liver tumors and to define the border between neoplastic and normal tissues. Here we report a 13-y-old female cynomolgus monkey with anorexia and serologically normal liver enzymes. After fluid therapy, the condition remained in remission for several months. Later, however, a palpable mass was assessed by using ultrasonography, radiology, and SPIO-MRI; T2-weighted images revealed a clear border between a hepatocellular carcinoma and normal liver tissue. Findings at necropsy supported the imaging data. Serologic assessment after euthanasia revealed a positive reaction to an abnormal form of prothrombin (PIVKA-II). We recommend SPIO-MRI as a practical and useful for diagnosing hepatocellular neoplasias in NHP. This study is the first to demonstrate the applicability of SPIO-MRI for the identification of hepatocellular carcinoma in NHP.

Abbreviations: HCC, hepatocellular carcinoma; SPIO, superparamagnetic iron oxide

DOI: 10.30802/AALAS-CM-17-000063

Superparamagnetic iron oxide (SPIO) is a liver-targeting MRI contrast agent that is absorbed by the reticuloendothelial system. Clinically approved SPIO agents are ferumoxides (Feridex, Bayer Healthcare, Wayne, NY) and ferucarbotran (Resovist, Bayer Healthcare) with particle sizes of 120 to 180 nm and about 60 nm, respectively. Both are used to improve the detectability of focal liver lesions, mainly by increasing tumor-to-liver contrast. Because metastatic liver cancers lack Kupffer cells, hepatic metastases do not take up SPIO, whereas normal phagocytic Kupffer cells in the reticuloendothelial system retain SPIO.[30] Consequently, T2 and T2* relaxation times significantly differ between normal tissue and lesions, such that lesions appear hypointense relative to the surrounding normal liver. This difference is useful for detecting metastatic liver cancer as areas of hypointensity. Residual Kupffer cells uptake SPIO in some tumors, including focal nodular hyperplasia, hepatic adenoma, well-differentiated hepatocellular carcinoma (HCC), and dysplastic nodules, indicating that SPIO-MRI can facilitate the radiologic differentiation of primary liver tumors.[11,12,18] Spontaneous neoplasias that rarely arise in NHP are unrelated to carcinogenic factors such as aflatoxin B1.[1,15,28] A previous study identified a relatively low incidence of spontaneous malignant tumors in cynomolgus (1.9%) and rhesus (3.8%) macaques.[29] The incidence is the lowest (1.4%) in rhesus macaque younger than 5 y, and 78.3% of all neoplasms have been diagnosed in monkeys older than 20 y. In fact, cancer contributes to 50% of all deaths among rhesus macaques older than 26 y,[25] and recent reports indicate that the number of tumors is increasing among elderly NHP.[3,6] This correlation between age and neoplasia has been recognized in other species.[8] However, primary hepatic tumors are still quite rare in NHP[5,7,10] and humans,[2,9,31] with the notable exception of prosimians, especially the Lemuridae,[24] in which spontaneous neoplasms can develop in the liver.[14,20] Hepatic iron, copper, and molybdenum are not associated with HCC in lemurs, suggesting that iron is not a key element in the pathogenesis of liver tumor formation.[34] Furthermore, metastatic spread from the liver to multiple abdominal organs is infrequent.[14,23] Borders between masses and normal organs are often—but not always—difficult to evaluate by radiography or ultrasonography.[16,22] However, as we mentioned previously, SPIO-MRI can noninvasively identify the size and location of tumors as

Received: 08 Jul 2017. Revision requested: 14 Aug 2017. Accepted: 04 Dec 2017.
[1]Tsukuba Primate Research Center, National Institutes of Biomedical Innovation, Health and Nutrition, Ibaraki, Japan; [2]College of Bioresource Science, Nihon University, Kanagawa, Japan; and [3]Corporation for Production and Research of Laboratory Primates, Ibaraki, Japan
[*]Corresponding author. Email: ageyama@nibiohn.go.jp

well as borders between tumors and normal liver tissues.[4] The most recent recommendations from the American Association for the Study of Liver Diseases state that HCC can be diagnosed when a mass larger than 2 cm shows typical features of HCC with contrast material, and SPIO-MRI is useful for masses measuring 1 to 2 cm.[32] The radiologic criteria favoring malignancy are size larger than 2 cm, hyperintensity on T2-weighted images, delayed hypointensity 'washout,' delayed enhancement of tumor capsule, and rapid interval growth.[32] However, the diagnostic application of MRI to live cynomolgus monkeys has not been reported. Here, we investigated the practical utility of SPIO-MRI for diagnosing hepatocellular neoplasia in NHP.

Materials and Methods

Clinical symptoms and clinical course. A 13-y-old female cynomolgus monkey had been bred and individually housed in accordance with the *Guide for the Care and Use of Laboratory Animals* in a stainless steel cage with visual and olfactory contact with other macaques under conditions of a temperature range of 23 to 27 °C, humidity of 50% to 70%, 12 air changes hourly, a 12:12-h light:dark cycle and was fed 70 g of commercial monkey chow (Type AS, Oriental Yeast, Chiba, Japan) and 100 g of fruit daily at the Tsukuba Primate Center.[13] The Animal Welfare and Animal Care Committee of the National Institutes of Biomedical Innovation, Health, and Nutrition (NIBIOHN, Osaka, Japan) approved the experimental protocol. This monkey had been healthy except for being obese, without signs of disease at annual health examinations, and levels of liver enzymes (ALT and AST) were normal. She was certified free of simian retrovirus type D, herpesvirus B, simian varicella virus, and SIV and had never been used for experimentation.

She developed anorexia and mild weight loss, which initially was alleviated by fluid therapy. However, several months after apparent recovery, laboratory analysis of serum parameters (AU480 Chemistry System, Beckman Coulter, Brea, CA) revealed elevated values for creatinine (1.8 mg/dL; normal reference value, 0.8 ± 0.1 mg/dL) and ALP (1924 IU/L; normal reference value, 453 ± 179 IU/L). At that time, firm, palpable masses were discovered within the upper abdomen. Ultrasonography (data not shown) and plain radiology (Figure 1) suggested the presence of liver masses and an associated pulmonary mass. Contrast-enhanced noninvasive SPIO-MRI revealed several masses in the liver.

General anesthesia was induced by using ketamine hydrochloride (10 mg/kg IM; Ketalar, Daiichi Sankyo Propharma, Tokyo, Japan) and maintained by mask anesthesia with isoflurane gas (2%; Pfizer, New York, NY). Subsequent exploratory laparotomy revealed massive neoplasms that were deemed too difficult to resect because of their location and the extent of infiltration. After exploratory laparotomy, cefazolin sodium hydrate (50 mg/kg IM; Cefamezin α, Astellas Pharma, Tokyo, Japan) was administered to prevent infection, and buprenorphine hydrochloride (0.02 mg/kg IM, Zalban, Nissin Pharmaceutical, Yamagata, Japan) was administered for analgesia.

Several days later, the macaque was euthanized by using sodium pentobarbital overdose because of a poor prognosis. Biochemical findings revealed that the animal had been negative for serum α-fetoprotein[27] and positive for the PIVKA-II protein,[33] both of which are hepatic tumor markers in NHP.

Figure 1. Plain-film radiographic images acquired after confirming serologic abnormalities. White arrows, liver masses and associated pulmonary metastasis.

Enhanced MRI. After unenhanced MRI of the abdomen, SPIO contrast-enhanced MR images of the liver were acquired (Allegra 3-T scanner, Siemens, Munich, Germany). The macaque was intubated and mechanically ventilated (ADS1000, Shin-ei, Tokyo, Japan) under general anesthesia with ketamine hydrochloride and isoflurane gas during 3-T MR image acquisition. Single boluses of SPIO agent (0.45 mg Fe/kg; Resovist, Bayer Schering Pharma, Berlin, Germany) were administered through a saphenous vein. Enhanced images were acquired after 10 to 15 min. T2-weighted images were acquired under the following parameters: repetition time, 2500 ms; echo time, 90 ms, fractional anisotropy, 90°; and slice thickness, 2.5 mm. In addition, the macaque was assessed in the dorsal position by using a head coil for ECG and respiratory gating.

Histopathologic analysis. The liver and lung tissues were fixed in 10% neutral buffered formalin, processed routinely, and embedded in paraffin wax. Sections (3 mm) were stained with hematoxylin and eosin, periodic acid–Schiff, and silver. In addition, neoplastic cells underwent immunohistochemistry. Sections were dewaxed and immersed in 0.5% H_2O_2 in methanol, and antigen was retrieved by using citric acid buffer (pH 6.0). The sections were placed in an autoclave for 10 min at 121 °C and then incubated overnight at 4 °C with primary mouse monoclonal antibodies specific for cytokeratin 7 (dilution, 1:50; CK7, Dako, Glostrup, Denmark), cytokeratin 20 (1:200; CK20, Dako), surfactant protein A (1:100; SP-A, Dako), hepatocytes (1:50; Dako), and vimentin (1:50; Dako). The sections were briefly washed with buffer and incubated in the EnVision+ Dual Link HRP System (Dako) for 30 min. Labeling

was visualized by immersing the sections in the chromogen DAB (Dojin Kagaku, Tokyo, Japan) and H_2O_2[23] and counterstaining with hematoxylin.

Results

MR images. In our cynomolgus macaque, the border between the hepatocellular neoplasia and the normal liver was rendered more clearly on T2- than T1-weighted images (white arrows, Figure 2 A and B, respectively). Neoplastic cells were scarce among Kupffer cells and did not uptake SPIO particles. Therefore, after SPIO infusion, neoplasias appeared hyperintense against the normal, dark background of the liver.

Macroscopic findings. At the time of necropsy, the macaque's weight had decreased from 5.26 to 3.95 kg over a period of 6 mo, and the animal seemed somewhat emaciated. Macroscopic findings revealed 3 masses in the right medial hepatic lobe (Figure 3 A) and a larger mass (diameter, 5 cm) in the left lateral hepatic lobe. On cut section, these masses were greenish yellow and the center was yellowish white, due to necrosis (Figure 3 B). The gallbladder was extremely enlarged with soluble, greenish-black bile. Dark-green or brownish-red, multinodular neoplasms measuring $7 \times 8 \times 4$ cm were found at the base of the anterior lobe of the left lung and in the medial and posterior lobes (Figure 3 C). Many dark-red nodules (diameter, less than 1 cm) had spread throughout the right lung lobes. Several tight adhesions were identified between the dorsal aspect of the left lung and thorax and between the right lateral hepatic lobe and right kidney.

Histopathologic analyses. Histopathology revealed extensive infiltration of the liver by atypical neoplastic cells that were pleomorphic and minimally cohesive, with a large oval or pleomorphic macronucleus or were multinucleated with prominent nucleoli. Abnormal nuclear divisions and Mallory bodies were predominant among the atypical cells (Figure 4 A), which did not produce bile. Liver staining with periodic acid–Schiff revealed round cytoplasmic globular inclusions that resembled globular hyaline bodies in some neoplastic cells (Figure 4 B); silver impregnation demonstrated decreased reticulin fibers in these lesions (data not shown). The neoplastic cells were immunocytochemically negative for CK7, CK20, surfactant protein A, and vimentin (data not shown). Some atypical cells stained weakly positive with antihepatocyte antibody (data not shown). In addition, the lungs had been extensively infiltrated by neoplastic cells that were similar to those in the liver (Figure 5). Neoplastic thrombi were found in some liver and lung vessels. Poorly differentiated HCC-like neoplasia and pulmonary metastases were diagnosed in light of these findings.

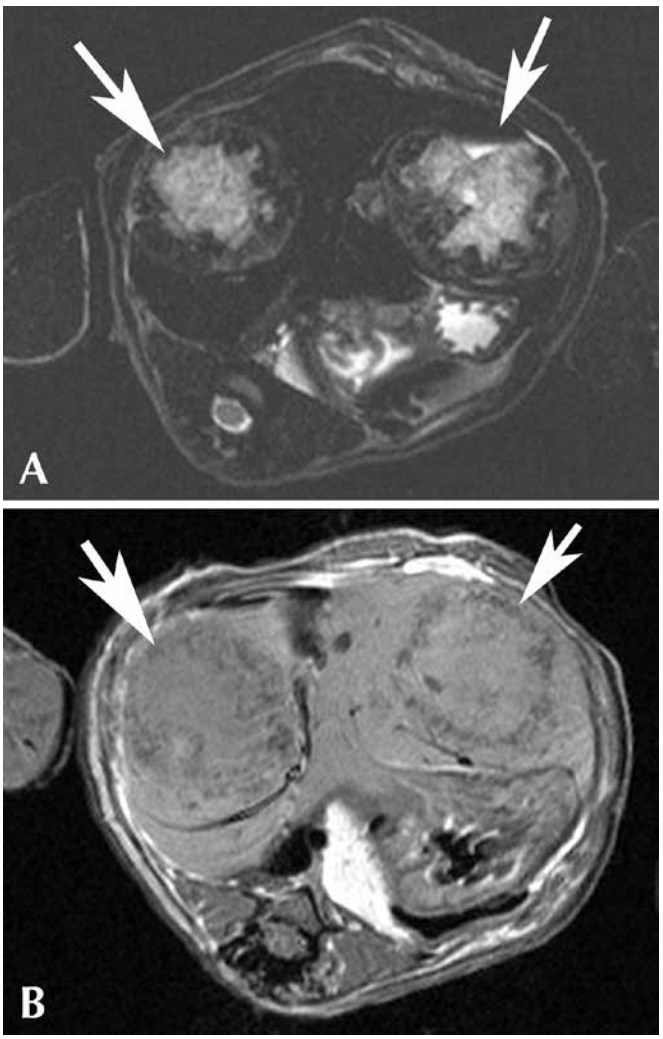

Figure 2. MR images acquired by using a 3-T scanner with SPIO contrast enhancement. The border between hepatocellular neoplasia (white arrow) and normal liver is delineated more effectively on (A) T2- than (B) T1-weighted imaging.

Discussion

Ferucarbotran consists of 60-nm SPIO nanoparticles and a contrast agent with 4- to 5-nm crystals. The particles are coated with dextran and attached through electrostatic interaction to the iron core by hydrogen bonds between hydroxyl groups on the dextran and oxide groups on the surface of the iron core. An unattached dextran tail covers the remaining iron crystals and contributes to most of the hydrodynamic diameter of the SPIO nanoparticles.[17] We selected ferucarbotran for this study because it can be administered as a rapid bolus. On ferucarbotran-enhanced MR images, organs with neoplasia appear brighter than normal organs because Kupffer cells in normal organs phagocytize SPIO nanoparticles. The contrast on such MR images renders hepatocellular neoplasia easy to diagnose. Liver tumors appeared markedly brighter than other sites on T2-weighted MR images (Figure 2 A). Although SPIO-MRI is useful for diagnosing metastasis of hepatocellular neoplasia,[18] whether it can be used to discriminate pulmonary or bone metastasis has not yet been reported. Metastasis in the lungs or bone might be undetectable by SPIO-MRI, including our system, because of a lack of macrophages or due to the target organ's function. From the perspective of serologic analysis, PIVKA-II values have already been established as practical indicators of HCC in NHP. We confirmed that the PIVKA-II value in the macaque we present indicated HCC.[33] Several reports have described both α-fetoprotein-positive[21] and -negative[1,23] HCC in NHP. Increasing serum α-fetoprotein values in humans indicate cirrhosis or hepatitis and may not necessarily increase due to HCC.[19,26] Opinions about α-fetoprotein-negative and -positive HCC conflict, and the matter is difficult to resolve because few NHP with HCC have been studied. Some neoplastic cells in the macaque we described here had Mallory or globular hyaline bodies, and some cells were weakly positive for antihepatocyte antibody (Figure 4 A and B). Therefore, a poorly

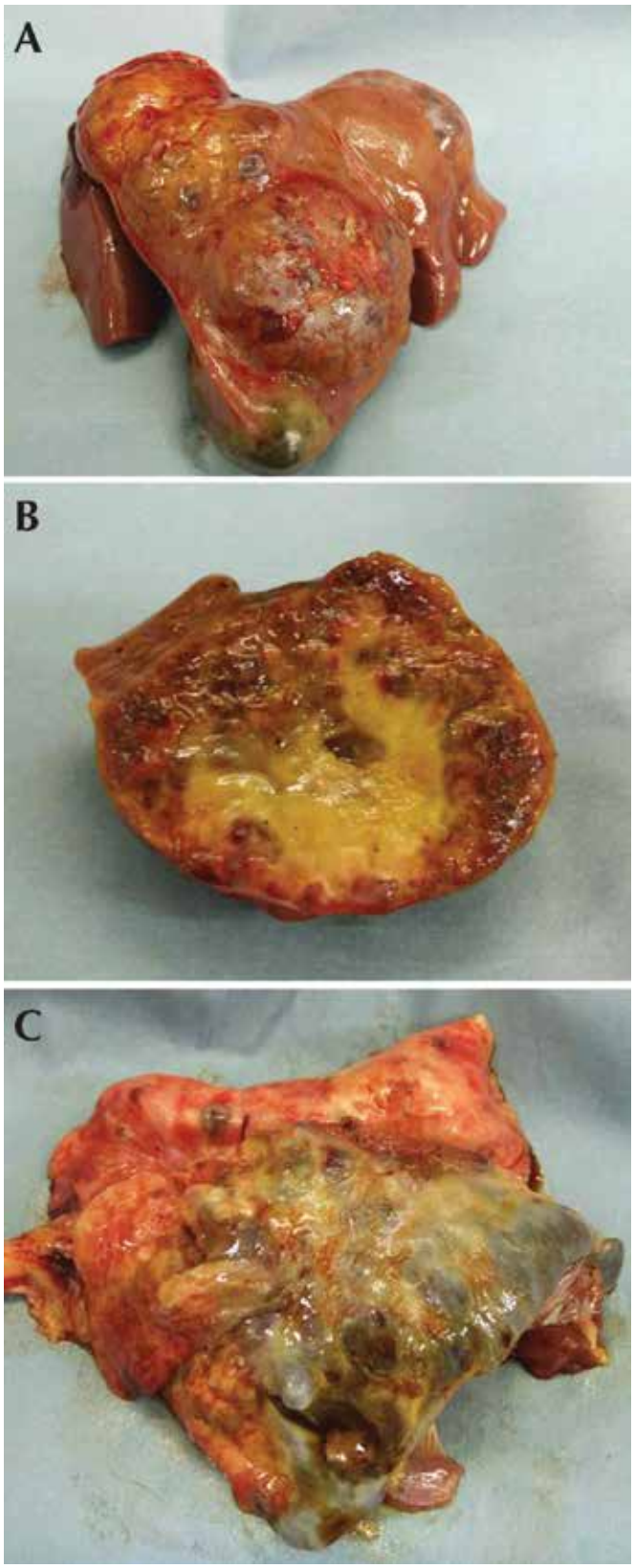

Figure 3. Macroscopic findings from liver and lung. (A) Three large masses are located in the medial hepatic lobe. (B) The cut surface of the mass is greenish yellow and the center has yellowish-white regions due to necrosis. (C) Dark-green or brownish-red multinodular neoplasms measuring 7 × 8 × 4 cm are located at the base of the anterior lobe of the left lung and in the medial and posterior lobes.

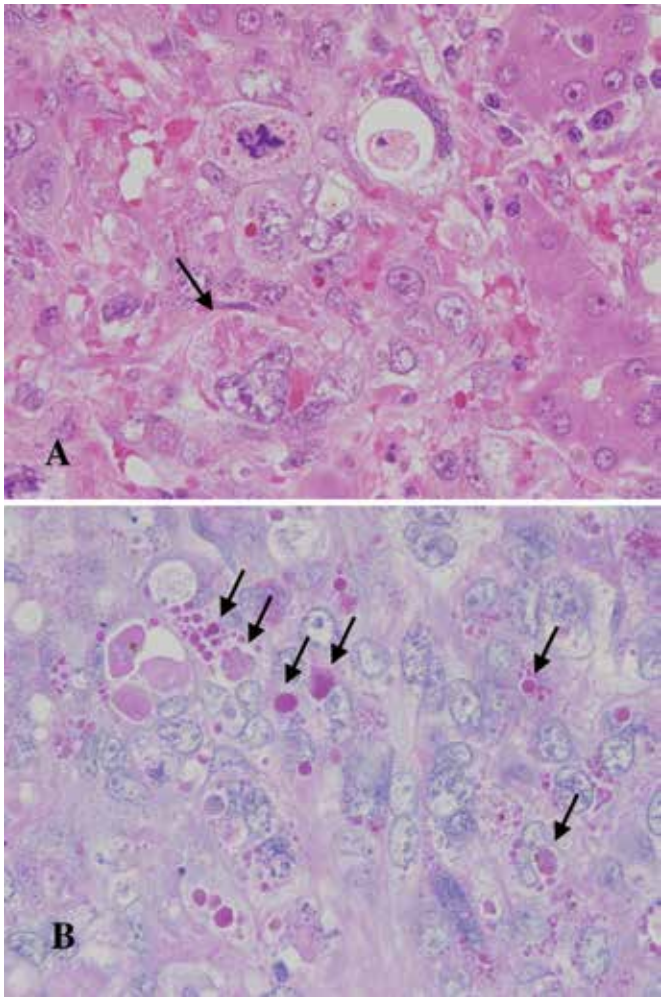

Figure 4. Histologic findings from liver. The neoplastic cells have large, oval, atypical nuclei or pleomorphic macronuclei with prominent nucleoli (arrow). Some neoplastic cells had abnormal nuclear division and Mallory bodies. Hematoxylin and eosin stain; magnification, 400×. (B) Staining with periodic acid–Schiff shows round cytoplasmic globular inclusions (arrows) resembling globular hyaline bodies in some neoplastic cells. Magnification, 400×.

differentiated HCC-like neoplasia was diagnosed in light of the histopathologic findings and other clinical background parameters.

The SPIO-MRI method is noninvasive and free of undesirable side effects. To our knowledge, findings from enhanced MRI and postmortem imaging in NHP have not been compared previously. This report delivers additional information about HCC in cynomolgus macaques, which therefore likely is valuable in terms of their care and use as research models. In addition, we hope to improve the enhanced MRI procedure to assess responses to anticancer therapies in cynomolgus macaques. This report is the first to demonstrate the applicability of SPIO-MRI for diagnosing HCC in NHP.

Acknowledgments

We thank Hiromi Ogawa and Hayato Narita for assistance with the clinical procedures and Chieko Ohno for help with the pathologic assessment. This study was supported by JSPS KAKENHI (grant nos. 17790515, 24615009, and 15K07789) as well as by grants from the Japan Agency for Medical Research and Development.

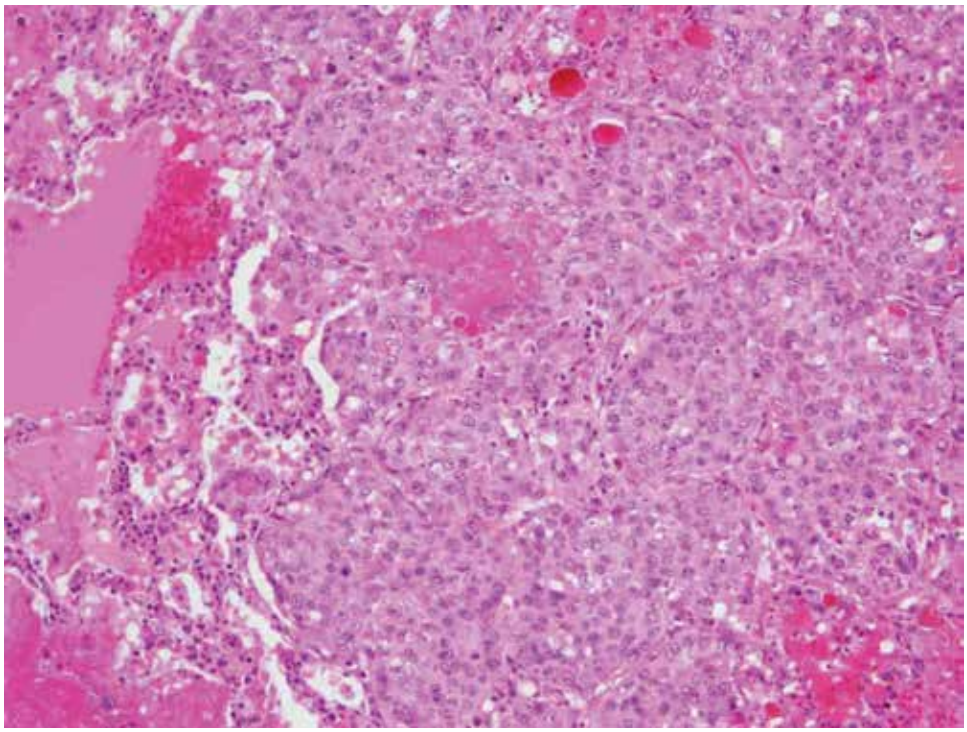

Figure 5. Histologic findings from lung. Lungs are extensively infiltrated by neoplastic cells similar to those in the liver. Hematoxylin and eosin stain; magnification, 100×.

References

1. **Adamson RH, Correa P, Sieber SM, Mclntire KR, Dalgard DW.** 1976. Carcinogenicity of aflatoxin B1 in rhesus monkeys: 2 additional cases of primary liver cancer. J Natl Cancer Inst **57:**67–78. https://doi.org/10.1093/jnci/57.1.67.
2. **Anderson BB, Ukah F, Tette A, Villaflor SG, Koh D, Seton P.** 1992. Primary tumors of the liver. J Natl Med Assoc **84:**129–135.
3. **Beniashvili DS.** 1989. An overview of the world literature on spontaneous tumors in nonhuman primates. J Med Primatol **18:**423–437.
4. **Benveniste H, Fowler JS, Rooney WD, Moller DH, Backus WW, Warner DA, Carter P, King P, Scharf B, Alexoff DA, Ma Y, Vaska P, Schlyer D, Volkow ND, PET study; MRI study.** 2003. Maternal-fetal in vivo imaging: a combined PET and MRI study. J Nucl Med **44:**1522–1530.
5. **Borda JT, Ruiz JC, Sanchez-Negrette M.** 1996. Spontaneous hepatocellular carcinoma in *Saimiri boliviensis*. Vet Pathol **33:**724–726. https://doi.org/10.1177/030098589603300617.
6. **Brown SL, Anderson DC, Dick EJ Jr, Guardado-Mendoza R, Garcia AP, Hubbard GB.** 2009. Neoplasia in the chimpanzee (*Pan* spp.). J Med Primatol **38:**137–144. https://doi.org/10.1111/j.1600-0684.2008.00321.x.
7. **Cianciolo RE, Butler SD, Eggers JS, Dick EJ Jr, Leland MM, de la Garza M, Brasky KM, Cummins LB, Hubbard GB.** 2007. Spontaneous neoplasia in the baboon (*Papio* spp.). J Med Primatol **36:**61–79. https://doi.org/10.1111/j.1600-0684.2006.00202.x.
8. **DePaoli A, McClure HM.** 1982. Gastrointestinal neoplasms in NHPs: a review and report 11 new cases. Vet Pathol Suppl **7:**104–125. https://doi.org/10.1177/030098588201907s08.
9. **Forbes A, Portmann B, Johnson P, Williams R.** 1987. Hepatic sarcomas in adults: a review of 25 cases. Gut **28:**668–674. https://doi.org/10.1136/gut.28.6.668.
10. **Fujishima J, Satake S, Furukawa T, Kurokawa C, Kodama R, Moriyama A, Sasaki Y, Kamimura Y, Maeda H.** 2011. Focal nodular hyperplasia in the livers of cynomolgus macaques (*Macaca fascicularis*). J Toxicol Pathol **24:**125–129. https://doi.org/10.1293/tox.24.125.
11. **Grandin C, Van Beers BE, Robert A, Gigot JF, Geubel A, Pringot J.** 1995. Benign hepatocellular tumors: MRI after superparamagnetic iron oxide administration. J Comput Assist Tomogr **19:**412–418. https://doi.org/10.1097/00004728-199505000-00014.
12. **Imai Y, Murakami T, Yoshida S, Nishikawa M, Ohsawa M, Tokunaga K, Murata M, Shibata K, Zushi S, Kurokawa M, Yonezawa T, Kawata S, Takamura M, Nagano H, Sakon M, Monden M, Wakawa K, Nakamura H.** 2000. Superparamagnetic iron oxide-enhanced magnetic resonance images of hepatocellular carcinoma: correlation with histological grading. Hepatology **32:**205–212. https://doi.org/10.1053/jhep.2000.9113.
13. **Institute for Laboratory Animal Research.** 2011. Guide for the care and use of laboratory animals, 8th ed. Washington (DC): National Academies Press.
14. **Laing ST, Lemoy MJ, Sammak RL, Tarara RP.** 2013. Metastatic hepatocellular carcinoma in a juvenile rhesus macaque (*Macaca mulatta*). Comp Med **63:**448–453.
15. **Lang CD, Daviau JS, Merton DA, Caraker SM.** 2013. Adenocarcinoma of the illeocolic junction and multifocal hepatic sarcoma in an aged rhesus macaque (*Macaca mulatta*). Comp Med **63:**361–366.
16. **Long CT, Luong RH, McKeon GP, Albertelli M.** 2010. Uterine leiomyoma in a Guyanese squirrel monkey (*Saimiri sciureus sciureus*). J Am Assoc Lab Anim Sci **49:**226–230.
17. **Modo MMJ, Bulte JWM.** 2007. Molecular and cellular MR imaging. Boca Raton (FL): CRC Press https://doi.org/10.1201/9781420004090
18. **Nishie A, Tajima T, Ishigami K, Ushijima Y, Okamoto D, Hirakawa M, Nishihara Y, Taketomi A, Hatakenaka M, Irie H, Yoshimitsu K, Honda H.** 2010. Detection of hepatocellular carcinoma (HCC) using super paramagnetic iron oxide (SPIO)-enhanced MRI: added value of diffusion-weighted imaging (DWI). J Magn Reson Imaging **31:**373–382. https://doi.org/10.1002/jmri.22059.
19. **Patil M, Sheth KA, Adarsh CK.** 2013. Elevated α fetoprotein, no hepatocellular carcinoma. J Clin Exp Hepatol **3:**162–164. https://doi.org/10.1016/j.jceh.2013.02.246
20. **Porter BF, Goens SD, Brasky KM, Hubbard GB.** 2004. A case report of hepatocellular carcinoma and focal nodular hyperplasia with a myelolipoma in 2 chimpanzees and a review of spontaneous hepatobiliary tumors in nonhuman primates. J Med Primatol **33:**38–47. https://doi.org/10.1111/j.1600-0684.2003.00048.x.
21. **Princler GL, Mclntire KR, Adamson RH.** 1978. In vitro α-fetoprotein synthesis by monkey hepatocellular carcinoma. J Natl Cancer Inst **60:**643–648. https://doi.org/10.1093/jnci/60.3.643.

22. **Rajiah P, Sinha R, Cuevas C, Dubinsky TJ, Bush WH Jr, Kolokythas O.** 2011. Imaging of uncommon retroperitoneal masses. Radiographics **31:**949–976. https://doi.org/10.1148/rg.314095132.
23. **Reindel JF, Walsh KM, Toy KA, Bobrowski WF.** 2000. Spontaneously occurring hepatocellular neoplasia in adolescent cynomolgus monkeys (*Macaca fascicularis*). Vet Pathol **37:**656–662. https://doi.org/10.1354/vp.37-6-656.
24. **Remick AK, Van Wettere AJ, Williams CV.** 2009. Neoplasia in prosimians: case series from a captive prosimian population and literature review. Vet Pathol **46:**746–772. https://doi.org/10.1354/vp.08-VP-0154-R-FL.
25. **Simmons HA, Mattison JA.** 2011. The incidence of spontaneous neoplasia in 2 populations of captive rhesus macaques (*Macaca mulatta*). Antioxid Redox Signal **14:**221–227. https://doi.org/10.1089/ars.2010.3311.
26. **Snowberger N, Chinnakotla S, Lepe RM, Peattie J, Goldstein R, Klintmalm GB, Davis GL.** 2007. α-Fetoprotein, ultrasound, computerized tomography, and magnetic resonance imaging for detection of hepatocellular carcinoma in patients with advanced cirrhosis. Aliment Pharmacol Ther **26:** 1187–1194. https://doi.org/10.1111/j.1365-2036.2007.03498.x
27. **Souza e Silva IS, Gonzåles AM, Linhares MM, Salzedas Neto A, Szejnfeld D, D'ippolito G, Lopes Filho Gde J, Lanzoni VP, Matos CA.** 2013. Long-term follow-up after resection of thyroid metastases from hepatocellular carcinoma in noncirrhotic liver. Arq Bras Endocrinol Metabol **57:**327–331. https://doi.org/10.1590/S0004-27302013000400009.
28. **Sieber SM, Correa P, Dalgard DW, Adamson RH.** 1979. Induction of osteogenic sarcomas and tumors of the hepatobiliary system in NHPs with aflatoxin B1. Cancer Res **39:**4545–4554.
29. **Takayama S, Thorgeirsson UP, Adamson RH.** 2008. Chemical carcinogenesis studies in nonhuman primates. Proc Jpn Acad Ser B Phys Biol Sci **84:**176–188. https://doi.org/10.2183/pjab.84.176.
30. **Wang YX.** 2011. Superparamagnetic iron oxide based MRI contrast agents: Current status of clinical application. Quant Imaging Med Surg **1:**35–40.
31. **Weitz J, Klimstra DS, Cymes K, Jarnagin WR, D'Angelica M, La Quaglia MP, Fong Y, Brennan MF, Blumgart LH, Dematteo RP.** 2007. Management of primary liver sarcomas. Cancer **109:**1391–1396. https://doi.org/10.1002/cncr.22530.
32. **Willatt JM, Hussain HK, Adusumilli S, Marrero JA.** 2008. MR imaging of hepatocellular carcinoma in the cirrhotic liver: challenges and controversies. Radiology **247:**311–330. https://doi.org/10.1148/radiol.2472061331.
33. **Yoshizawa K, Oishi Y, Sano K, Tsubota K, Ikeda K, Fukuhara Y, Senzaki H, Tsubura A.** 2002. Hepatocellular carcinoma with PIVKA-II production in a young laboratory monkey. J Toxicol Pathol **15:**61–68. https://doi.org/10.1293/tox.15.61.
34. **Zadrozny LM, Williams CV, Remick AK, Cullen JM.** 2009. Spontaneous hepatocellular carcinoma in captive prosimians. Vet Pathol **47:**306–311. https://doi.org/10.1177/0300985809359380.